

# Observations of the pulsation of the Cepheid $\ell$ Car with the Sydney University Stellar Interferometer

J. Davis,<sup>\*</sup> A.P. Jacob, J.G. Robertson, M.J. Ireland, J.R. North, W.J. Tango and P.G. Tuthill

*Sydney Institute for Astronomy, School of Physics, University of Sydney, NSW 2006, Australia*

9 October 2018

## ABSTRACT

Observations of the southern Cepheid  $\ell$  Car to yield the mean angular diameter and angular pulsation amplitude have been made with the Sydney University Stellar Interferometer (SUSI) at a wavelength of 696 nm. The resulting mean limb-darkened angular diameter is  $2.990 \pm 0.017$  mas (i.e.  $\pm 0.6$  per cent) with a maximum-to-minimum amplitude of  $0.560 \pm 0.018$  mas corresponding to  $18.7 \pm 0.6$  per cent in the mean stellar diameter. Careful attention has been paid to uncertainties, including those in measurements, in the adopted calibrator angular diameters, in the projected values of visibility squared at zero baseline, and to systematic effects. No evidence was found for a circumstellar envelope at 696 nm. The interferometric results have been combined with radial displacements of the stellar atmosphere derived from selected radial velocity data taken from the literature to determine the distance and mean diameter of  $\ell$  Car. The distance is determined to be  $525 \pm 26$  pc and the mean radius  $169 \pm 8 R_{\odot}$ . Comparison with published values for the distance and mean radius show excellent agreement, particularly when a common scaling factor from observed radial velocity to pulsation velocity of the stellar atmosphere (the  $p$ -factor) is used.

**Key words:** Cepheids: general — stars: individual ( $\ell$  Car, HR 3884) — stars: distances — techniques: interferometric

## 1 INTRODUCTION

The accurate determination of the zero point of the Cepheid Period-Luminosity relation is an important step in the refinement of the extragalactic distance scale. The combination of interferometric and spectroscopic data, as discussed by Davis (1999), is an approach to this task that is now feasible. The first demonstration of the combination of interferometric and spectroscopic data to determine both the mean diameter and distance of a Cepheid was made by Lane et al. (2000) based on interferometric observations with the Palomar Testbed Interferometer (PTI) of  $\zeta$  Gem. Lane, Creech-Eakman & Nordgren (2002) subsequently applied the technique to  $\eta$  Aql and, with additional data, to  $\zeta$  Gem, again based on PTI observations. Kervella et al. (2004a) have reported the measurement of the angular pulsations of seven Galactic Cepheids made with the European Southern Observatory's Very Large Telescope Interferometer (VLTI) and, in combination with spectroscopic data, have determined the distances to the Cepheids.

One of the prime programmes for which the Sydney

University Stellar Interferometer (SUSI) (Davis et al. 1999) was developed was the measurement of the mean diameters and angular pulsation amplitudes of Cepheids but, in its initial configuration, it lacked the required sensitivity. The recent commissioning of a red beam-combination system in SUSI (Davis et al. 2007a) has resulted in a significant increase in sensitivity. In this paper we report SUSI measurements of the mean angular diameter and angular pulsation amplitude of  $\ell$  Car, one of the seven Cepheids measured with the VLTI by Kervella et al. (2004a). A preliminary analysis was presented at a European Southern Observatory symposium in 2005 (Davis et al. 2007b) and Jacob (2008) has discussed the SUSI Cepheid programme including an analysis of a subset of the  $\ell$  Car observations reported here.

Spectroscopic radial velocity measurements from the literature have been combined to produce a radial velocity versus pulsation phase curve and, after scaling with a fixed  $p$ -factor as discussed in Section 6.3, this has been integrated to give the radial displacement of the Cepheid surface as a function of pulsation phase. The radial displacement and limb-darkened angular diameter data have been combined to determine the distance and mean radius of  $\ell$  Car.

The resulting distance and mean radius are compared

<sup>\*</sup> E-mail: j.davis@physics.usyd.edu.au

with values in the literature determined by the same technique and by the infrared surface brightness method and excellent agreement is found, particularly when all values are scaled to a common  $p$ -factor.

## 2 THE PULSATION PHASE

Although it might seem premature to discuss the pulsation phase prior to discussing the observations it is necessary to ensure that both interferometric and spectroscopic phases are synchronised since the epochs of the interferometric and spectroscopic observations do not overlap. A problem in the case of  $\ell$  Car is the fact that there is evidence that its period has undergone changes. Szabados (1989) reported that the period of  $\ell$  Car changed from 35.5318 days prior to JD2440000 to 35.5513 days. Shobbrook (1992) refined the Szabados period, with additional photometry in 1990, to 35.5443 days and Berdnikov & Turner (2004), based on photometry in 2002, give a value of 35.5572 days. Taylor et al. (1997) have listed values back to 1901 and found in their own spectroscopic study of  $\ell$  Car from early 1991 to late 1996 that an increase in the period was evident although the uncertainties were large.

The approach that we have adopted is as follows. Since the largest body of radial velocity data available to us is the combined Mount Stromlo Observatory (MSO) and Mount John University Observatory (MJUO) observations analysed by Taylor et al. (1997) and their phases are effectively based on the Shobbrook (1992) ephemeris, albeit with small adjustments to bring the early MJUO data into line with the MSO data, we have adopted the Shobbrook (1992) ephemeris for the analysis of both interferometric and additional spectroscopic data. The adopted period is  $35.5443 \pm 0.0006$  days with  $2447880.81 \pm 0.10$  the zero point of maximum light in heliocentric Julian Date. The phases of individual data points have been computed from the Julian Date of observation for both interferometric and spectroscopic data.

Because of the variations in period it is found that there are small phase shifts between data sets taken at different epochs. The change in phase across any given data set as a result of adopting the Shobbrook period rather than for example, that of Berdnikov & Turner (2004), is negligible, and a small phase shift of the whole data set to bring it into alignment with the Taylor et al. (1997) data is justified. Details of the alignment of the different sets of data will be discussed when combining data and, in particular, spectroscopic data in Section 6.

## 3 THE INTERFEROMETRIC OBSERVATIONS

Measurements of the squared fringe visibility  $V^2$  were made with SUSI (Davis et al. 1999) using the red beam-combination system, which employs the fringe-scanning technique (Davis et al. 2007a). This beam-combination system uses matched filters with a central wavelength of 700 nm and spectral bandwidth of 80 nm. The observations to determine the angular diameter of  $\ell$  Car were made with a baseline of 40 m with additional measurements at 5 m to enable the zero baseline value of  $V^2$  to be checked.

**Table 1.** Calibrators used for the observations of  $\ell$  Car.  $m_{695}$  is the estimated magnitude at 695 nm,  $\theta_{UD}$  the adopted uniform disk angular diameter at 695 nm and  $\Omega$  the angular distance of the calibrator from  $\ell$  Car.

HR	Star	Spectral Type	$m_{695}$	$\theta_{UD}$ (mas)	$\Omega$ (deg)
3685	$\beta$ Car	A2 IV	1.6	$1.54 \pm 0.07$	7.9
3699	$\iota$ Car	A8 Ib	2.0	$1.55 \pm 0.12$	4.7
4114	s Car	F2 II	3.5	$0.90 \pm 0.07$	6.5

### 3.1 Calibrators

Calibrators were selected as close in the sky as possible to  $\ell$  Car with the additional requirement of being minimally resolved. The limiting sensitivity of SUSI at 700 nm is  $\sim +5$  which limited the choice of calibrators and compromise was necessary. The calibrators used are listed in Table 1 with their spectral types, adopted uniform-disk angular diameters, and angular distances from  $\ell$  Car. Common calibrators were used throughout to eliminate the potential influence of calibrator diameters on the pulsation curve. The effective wavelength of observations of all three calibrators has been estimated to be  $695.0 \pm 2.0$  nm following a similar analysis to that described by Davis et al. (2007a).

The uniform-disk angular diameters have been determined from measurements made with the Narrabri Stellar Intensity Interferometer (NSII) (Hanbury Brown, Davis & Allen 1974) and with the Mark III Optical Interferometer (Mark III) (Mozurkewich et al. 2003). In the case of  $\beta$  Car the value measured with the NSII has been adopted after correction from the limb-darkened angular diameter to the uniform-disk angular diameter using the appropriate correction factor for 695 nm interpolated from the tabulation of Davis, Tango & Booth (2000). In the absence of measured angular diameters for  $\iota$  and s Car, limb-darkened angular diameters have been determined by interpolation in a plot of NSII and Mark III limb-darkened angular diameters for unreddened visual magnitude  $V_0 = 0.0$  versus  $(B-V)_0$  for  $(B-V)_0 < 0.6$ . The interpolated limb-darkened angular diameters have been corrected to the  $V_0$  magnitudes of the stars and corrected for limb-darkening to give the uniform-disk angular diameters listed in Table 1, again using appropriate correction factors interpolated from the tabulation of Davis et al. (2000). The uncertainties in the uniform-disk angular diameters have been estimated from the scatter in the plot of limb-darkened angular diameters versus  $(B-V)_0$ .

### 3.2 The Observations

Observations of calibrators and  $\ell$  Car were alternated in each observing session so that every  $\ell$  Car observation was bracketed by observations of calibrators. Each observation consisted of a set of 1000 scans each 140  $\mu$ m long and consisting of 1024 by 0.2 ms samples. Each scan set was followed by photometric and dark scans. One complete observation of  $\ell$  Car, including the bracketing calibrators, took a total of  $\sim 18$  minutes.

Observations were made with a baseline of 40 m on 31 nights for  $\ell$  Car between 2 March 2004 and 24 May 2007.

Initially all 31 nights were included in the analysis but four nights were subsequently rejected when their values were found to lie more than four standard deviations from the fit to limb-darkened angular diameter versus radial displacement of the stellar surface (Section 7) and the analysis was then repeated without them. The maximum deviation from the fit after rejection of the four points was  $< 3.1\sigma$ . Examination of the data for three of the four rejected nights revealed that they were obtained during a short period in late March-early April 2004 when there was significant leakage of the metrology laser light into the signal beams. On the fourth rejected night, the data were poor, showing large scatter with only two out of the six points lying within one standard deviation of the mean for the night.

The projected baseline (i.e. the effective baseline of an observation) was less than 40 m due to the southerly declinations of  $\ell$  Car and its calibrators.

Observations were also made with a 5 m baseline, close to the phases of maximum and minimum angular diameter, on 13 March and 5 May 2007. These will be discussed in Section 5.1.

#### 4 ANALYSIS OF INTERFEROMETRY

The initial analysis of the fringe scans for  $\ell$  Car and the calibrators was carried out in the SUSI software “pipeline” (Davis et al. 2007a) which outputs the raw and seeing corrected squared visibility amplitudes ( $V^2$ ), the Julian Date, projected baseline, hour angle, fluxes etc. for each set of scans. For the early observations up to 7 April 2004 full sets of photometry files were not recorded. In these cases photometry files were duplicated to enable the scans to be processed in the pipeline and it is noted that analysis has shown that this procedure has a negligible effect on the resulting values of  $V^2$ . For each night the output file from the pipeline was imported into an Excel spreadsheet for examination of the data and for further analysis.

For each set of calibrator scans a Transfer Function ( $T$ ) was calculated.  $T$  is given by

$$T = \frac{V_{\text{obs}}^2}{V_{\text{exp}}^2} \quad (1)$$

where  $V_{\text{obs}}^2$  is the observed, seeing corrected value of  $V^2$  and  $V_{\text{exp}}^2$  is the expected value of  $V^2$  calculated from the uniform-disk angular diameter, effective wavelength and projected baseline.

The values of  $V_{\text{obs}}^2$  for  $\ell$  Car were then multiplied by the weighted mean value of  $T$  for the two calibrators bracketing the  $\ell$  Car observation to give the ‘true’ calibrated value of  $V^2$  for  $\ell$  Car. That is

$$V_{\text{true}}^2(\ell \text{ Car}) = \frac{V_{\text{obs}}^2(\ell \text{ Car})}{\bar{T}} \quad (2)$$

The mean value of  $V_{\text{true}}^2(\ell \text{ Car})$  for each night is listed in Table 2 with the date (Universal Time), the mean Julian Date (JD), the mean projected baseline, the calibrators used, and the number of scan sets for  $\ell$  Car. The uncertainty in  $V_{\text{true}}^2(\ell \text{ Car})$  takes into account the uncertainties in the uniform-disk angular diameters of the calibrators although these are generally negligible compared to the uncertainties in the values of  $V_{\text{obs}}^2$  for both calibrators and  $\ell$  Car.

**Table 2.** Calibrated values of  $V^2$ . The format for the date (Universal Time) is ddmmyy,  $\overline{\text{JD}}$  is the mean Julian Date of the observations minus 2450000,  $\bar{b}$  is the mean projected baseline, and  $\overline{V_{\text{true}}^2}(\ell \text{ Car})$  is the mean of  $N$  values of  $V_{\text{true}}^2(\ell \text{ Car})$ . Further details are given in the text.

Date	$\overline{\text{JD}}$	$\bar{b}$ (m)	$\overline{V_{\text{true}}^2}(\ell \text{ Car})$	Calibrators (Carinae)	N
020304	3067.039	33.72	0.388±0.020	$\beta$ & $\iota$	8
070304	3072.020	33.41	0.385±0.010	$\beta$ & $\iota$	8
170304	3081.940	33.49	0.274±0.013	$\beta$ & $\iota$	3
180304	3083.028	33.69	0.269±0.004	$\beta$ & $\iota$	3
010404	3096.964	33.67	0.301±0.014	$\beta$ & $\iota$	12
140404	3109.958	33.59	0.349±0.006	$\beta$ , $\iota$ & $s$	7
160404	3112.026	32.53	0.341±0.005	$\beta$ , $\iota$ & $s$	3
170404	3112.976	33.42	0.334±0.016	$\beta$ , $\iota$ & $s$	6
180404	3113.934	33.76	0.294±0.009	$\beta$ , $\iota$ & $s$	6
200404	3115.940	33.74	0.278±0.005	$\beta$ , $\iota$ & $s$	7
210404	3116.976	33.26	0.286±0.005	$\beta$ , $\iota$ & $s$	6
220404	3117.900	33.82	0.255±0.009	$\beta$ , $\iota$ & $s$	6
240404	3119.933	33.65	0.284±0.010	$\beta$ , $\iota$ & $s$	5
300404	3125.918	33.69	0.278±0.018	$\beta$ , $\iota$ & $s$	3
040504	3129.899	33.65	0.261±0.011	$\beta$ , $\iota$ & $s$	7
080504	3133.958	32.52	0.326±0.013	$\beta$ , $\iota$ & $s$	4
120504	3137.933	32.93	0.397±0.014	$\beta$ , $\iota$ & $s$	9
180105	3389.187	33.66	0.388±0.015	$\beta$ , $\iota$ & $s$	9
030205	3405.120	33.67	0.241±0.006	$\beta$ , $\iota$ & $s$	13
040205	3406.117	33.70	0.241±0.004	$\beta$ , $\iota$ & $s$	12
050205	3407.095	33.75	0.239±0.008	$\beta$ , $\iota$ & $s$	8
060205	3408.070	33.59	0.213±0.007	$\beta$ , $\iota$ & $s$	3
070205	3409.144	33.61	0.233±0.004	$\beta$ , $\iota$ & $s$	9
100205	3412.117	33.62	0.258±0.007	$\beta$ , $\iota$ & $s$	7
110205	3413.150	33.52	0.256±0.004	$\beta$ , $\iota$ & $s$	5
120205	3414.140	33.56	0.295±0.005	$\beta$ , $\iota$ & $s$	6
240507	4244.919	32.48	0.391±0.005	$\beta$ & $s$	7

#### 5 THE ANGULAR DIAMETER

The uniform-disk angular diameter ( $\theta_{\text{UD}}$ ) for each night was determined by fitting the equation

$$V^2 = \left| \frac{2J_1(x)}{x} \right|^2 \quad (3)$$

to the individual values of  $V_{\text{true}}^2(\ell \text{ Car})$  assuming that  $V_{\text{true}}^2(\ell \text{ Car})$  at zero baseline was unity. In equation (3)  $J_1(x)$  is a Bessel function and  $x = \pi b \theta_{\text{UD}} / \lambda$  where  $b$  is the projected baseline and  $\lambda$  is the wavelength of the observation.

The effective wavelength for  $\ell$  Car will be a function of pulsation phase as the star changes colour during its cycle. Calculations of effective wavelength for supergiants following the procedure described by Davis et al. (2007a) give the mean effective wavelength for  $\ell$  Car as 696.2 nm with a variation of  $\sim \pm 0.7$  nm, or  $\pm 0.1\%$ , over a complete pulsation cycle. The systematic uncertainty in the calculated effective wavelength is conservatively estimated to be  $\pm 2.0$  nm and we therefore adopt a fixed value of  $696.2 \pm 2.0$  nm as the effective wavelength for  $\ell$  Car. Since the expected variation is significantly less than the adopted uncertainty and, generally, small compared with the observational uncertainties in the angular diameters, the adoption of a fixed value is justified.

### 5.1 The Zero Baseline Value of $V_{\text{true}}^2(\ell \text{ Car})$

It is important to check the validity of the assumption that  $V_{\text{true}}^2(\ell \text{ Car})$  is unity at zero baseline. If it differs from unity as a result of the presence of a companion or scattered light from extended circumstellar matter, for example, it would translate to errors in the angular diameters. A large circumstellar envelope (CSE) has been discovered around  $\ell \text{ Car}$  at  $N$ -band using long-baseline interferometry by Kervella et al. (2006) and its signature was detected by the same authors in their  $K$ -band observations. CSEs have also been detected in the  $K$ -band around Polaris and  $\delta \text{ Cep}$  by Mérand et al. (2006) and around  $\text{Y Oph}$  by Mérand et al. (2007). Nardetto et al. (2008) confirm a dominant absorption component in  $\text{H}\alpha$  for  $\ell \text{ Car}$ , whose velocity is constant and near zero in the stellar rest frame, and they attribute this to a CSE. These detections of CSEs, particularly around  $\ell \text{ Car}$ , emphasise the importance of checking the validity of our assumption. In order to carry out this check, observations were made at a baseline of 5 m on 13 March 2007 at phase 0.023 and on 5 May 2007 at phase 0.514. The observations were therefore close to minimum and maximum angular diameter respectively. The observations were made after the initial analysis of the 40 m data had been completed so values for the uniform-disk angular diameter at the two phases could be interpolated from a plot of uniform-disk angular diameter versus phase. Given the angular diameter, and assuming  $V_{\text{true}}^2(\ell \text{ Car})$  to be unity at zero baseline, the expected value of  $V_{\text{true}}^2(\ell \text{ Car})$  at the projected baseline for each night was calculated. If the assumption that  $V_{\text{true}}^2(\ell \text{ Car})$  is unity at zero baseline is valid the observed and expected values will be in agreement. The results are listed in Table 3 and show that at minimum angular diameter the observed and expected values of  $V_{\text{true}}^2(\ell \text{ Car})$  differ by  $0.004 \pm 0.013$  and at maximum angular diameter by  $0.004 \pm 0.012$ . The assumption that  $V_{\text{true}}^2(\ell \text{ Car})$  is unity at zero baseline is therefore justified and there is no evidence of a significant effect of a CSE at 696 nm.

### 5.2 The Uniform-Disk Angular Diameters

The uniform-disk angular diameters corresponding to the dates of observation, together with the corresponding pulsation phases determined using the ephemeris of Shobbrook (1992) as discussed in Section 2, are listed in Table 4.

Figure 1 shows the data and fitted uniform-disk angular diameter curves for near minimum angular diameter (phase = 0.047 on 24 May 2007) and near maximum angular diameter (phase = 0.503 on 6 February 2005).

### 5.3 The Uniform-Disk Angular Diameter of the Calibrator $\iota \text{ Car}$

A check was made on the consistency of the transfer function  $T$  determined for the three primary calibrators, namely  $\beta$ ,  $\iota$  and  $s \text{ Car}$ . For each pair of consecutive observations of calibrators the transfer functions were plotted against each other. For example, where observations of  $\beta \text{ Car}$  and  $s \text{ Car}$  bracketed an observation of  $\ell \text{ Car}$ , the transfer function of  $\beta \text{ Car}$  was plotted against the transfer function of  $s \text{ Car}$ . For all the 40 m observations this resulted in 67 data points for  $s \text{ Car}$  v.  $\beta \text{ Car}$ , 85 points for  $\iota \text{ Car}$  v.  $\beta \text{ Car}$ , and 51 points

**Table 4.** The angular diameter of  $\ell \text{ Car}$ .  $\overline{\text{JD}}$  is the mean Julian Date of the observations minus 2450000 (see Table 2),  $\phi$  the mean pulsation phase for the observations,  $\theta_{\text{UD}}$  the uniform-disk angular diameter, Red.  $\chi^2$  the reduced  $\chi^2$  of the fit of equation (3) to the values of  $V_{\text{true}}^2(\ell \text{ Car})$ ,  $\rho_{696}$  the limb-darkening factor, and  $\theta_{\text{LD}}$  is the limb-darkened angular diameter. Further details are given in the text.

$\overline{\text{JD}}$	$\phi$	$\theta_{\text{UD}}$ (mas)	Red. $\chi^2$	$\rho_{696}$	$\theta_{\text{LD}}$ (mas)
3067.039	0.909	$2.575 \pm 0.052$	1.15	1.052	$2.709 \pm 0.055$
3072.020	0.049	$2.568 \pm 0.026$	0.73	1.049	$2.694 \pm 0.027$
3081.940	0.328	$2.933 \pm 0.031$	1.51	1.060	$3.109 \pm 0.033$
3083.028	0.359	$2.933 \pm 0.053$	0.02	1.060	$3.109 \pm 0.056$
3096.964	0.751	$2.814 \pm 0.016$	1.01	1.061	$2.986 \pm 0.017$
3109.958	0.116	$2.678 \pm 0.020$	0.61	1.051	$2.815 \pm 0.021$
3112.026	0.174	$2.787 \pm 0.031$	0.34	1.054	$2.937 \pm 0.033$
3112.976	0.201	$2.740 \pm 0.031$	1.90	1.055	$2.891 \pm 0.033$
3113.934	0.228	$2.850 \pm 0.044$	0.46	1.056	$3.010 \pm 0.046$
3115.940	0.284	$2.900 \pm 0.016$	0.82	1.058	$3.068 \pm 0.017$
3116.976	0.314	$2.914 \pm 0.015$	1.31	1.059	$3.086 \pm 0.016$
3117.900	0.340	$2.986 \pm 0.018$	2.28	1.060	$3.165 \pm 0.019$
3119.933	0.397	$2.889 \pm 0.048$	0.46	1.061	$3.065 \pm 0.051$
3125.918	0.565	$2.897 \pm 0.033$	3.61	1.063	$3.080 \pm 0.035$
3129.899	0.677	$2.909 \pm 0.015$	2.37	1.063	$3.092 \pm 0.016$
3133.958	0.791	$2.821 \pm 0.027$	4.16	1.059	$2.987 \pm 0.029$
3137.933	0.903	$2.564 \pm 0.024$	3.14	1.053	$2.697 \pm 0.025$
3389.187	0.972	$2.551 \pm 0.037$	0.99	1.049	$2.676 \pm 0.039$
3405.120	0.420	$3.056 \pm 0.023$	1.21	1.061	$3.242 \pm 0.024$
3406.117	0.448	$3.037 \pm 0.015$	0.97	1.062	$3.225 \pm 0.016$
3407.095	0.476	$3.056 \pm 0.025$	1.05	1.062	$3.245 \pm 0.027$
3408.070	0.503	$3.143 \pm 0.082$	0.19	1.062	$3.338 \pm 0.087$
3409.144	0.533	$3.071 \pm 0.026$	0.73	1.063	$3.264 \pm 0.028$
3412.117	0.617	$2.987 \pm 0.030$	0.44	1.063	$3.175 \pm 0.032$
3413.150	0.646	$2.978 \pm 0.032$	0.38	1.063	$3.166 \pm 0.034$
3414.140	0.674	$2.859 \pm 0.041$	0.10	1.063	$3.039 \pm 0.044$
4244.919	0.047	$2.613 \pm 0.020$	0.51	1.049	$2.741 \pm 0.021$

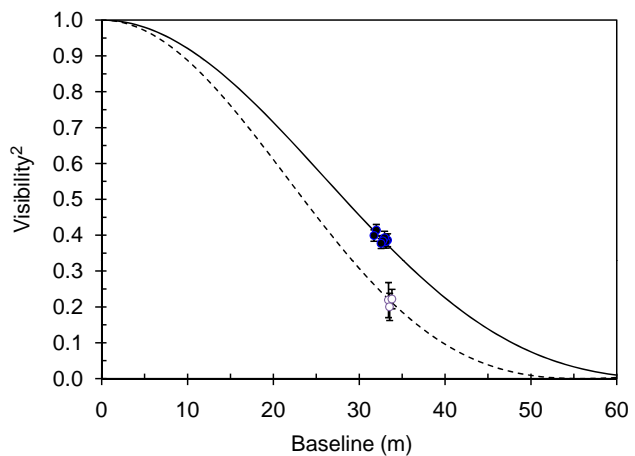


**Figure 1.** Examples of the data and fitted uniform-disk angular diameter curves for observations near minimum and maximum angular diameters. Key: The filled circles are the data for phase 0.047 on 24 May 2007 and the solid line is the fit to these data; the open circles are the data for phase 0.503 on 6 February 2005 and the dashed line is the fit to these data. Details of the fitting procedure are given in the text.

**Table 3.** The results of the 5 m observations near minimum and maximum values of the angular diameter of  $\ell$  Car. The format for the date is ddmmyy,  $\overline{JD}$  is the mean Julian Date of the observations minus 2450000,  $\phi$  the mean pulsation phase for the observations,  $\theta_{UD}$  is the estimated uniform-disk angular diameter,  $\overline{b}$  the mean baseline of the observations,  $V_{exp}^2$  the expected value of  $V^2$  for the uniform-disk angular diameter, baseline and effective wavelength (696.2 nm),  $V_{obs}^2$  is the mean value of the N observed values of  $V^2$ , and  $(V_{exp}^2 - V_{obs}^2)$  is the difference between the expected and observed values of  $V^2$ . Further details are given in the text.

Date	$\overline{JD}$	$\phi$	$\theta_{UD}$ (mas)	$\overline{b}$ (m)	$V_{exp}^2$	$V_{obs}^2$	N	$(V_{exp}^2 - V_{obs}^2)$
130307	4172.984	0.023	2.62±0.01	4.21	0.9855±0.0001	0.990±0.013	5	0.004±0.013
050507	4225.968	0.514	3.13±0.01	4.08	0.9806±0.0001	0.985±0.012	8	0.004±0.012

for  $\iota$  Car v. s Car. Linear regression fits of the form  $y = bx$  were made to each of the three plots.

In the case of s Car v.  $\beta$  Car,  $b = 1.001 \pm 0.006$  indicating that these two calibrators are consistent with each other. However, in the case of  $\iota$  Car v.  $\beta$  Car,  $b = 0.898 \pm 0.007$ , and for  $\iota$  Car v. s Car,  $b = 0.897 \pm 0.009$ . Since both these latter two plots show essentially the same slope, which differs significantly from the value of unity expected if the calibrators were consistent, it suggests that the value adopted for the uniform-disk angular diameter of  $\iota$  Car is too small. One possibility for this inconsistency is that  $\iota$  Car is a binary system but there is no evidence in the literature to support this. A careful examination of the SUSI data for the signature variations expected from a binary system has proved negative. It appears that the value adopted for the uniform-disk angular diameter is too small. Although it is hard to justify, arbitrarily increasing the angular diameter of  $\iota$  Car to  $1.77 \pm 0.12$  mas,  $\sim 2\sigma$  greater than predicted, gives  $b$  values closest to unity for  $\iota$  Car v.  $\beta$  Car and  $\iota$  Car v. s Car ( $b = 1.001 \pm 0.011$  for  $\iota$  Car v. s Car and  $b = 1.003 \pm 0.009$  for  $\iota$  Car v.  $\beta$  Car). The implications of making this change to the value of the uniform-disk angular diameter of  $\iota$  Car will be discussed in Section 8 but the analysis will initially be completed with the data in Table 4 which is based on the uniform-disk angular diameter of  $\iota$  Car being equal to  $1.55 \pm 0.12$  mas.

#### 5.4 Limb-Darkening Factors

In order to determine the true, limb-darkened angular diameters, the uniform-disk angular diameters have to be multiplied by limb-darkening factors ( $\rho_\lambda$ ) that are dependent on the centre-to-limb (CTL) intensity distributions for the star. The CTL intensity distributions are dependent on wavelength, and on the effective temperature ( $T_{eff}$ ), surface gravity ( $\log g$ ) and composition ( $[Fe/H]$ ) of the stellar atmosphere.

The form of the CTL intensity distribution and its phase dependence has been questioned. Marengo et al. (2002, 2003) have computed centre-to-limb intensity distributions for the Cepheid  $\zeta$  Gem and shown that their distributions computed for hydrodynamic models in spherical geometry differ from those for hydrostatic, plane-parallel models, particularly at certain ranges in phase. Nardetto et al. (2006b) have used a hydrodynamic model of  $\delta$  Cep to derive intensity distributions in the continuum and in four spectral lines. They found that limb-darkening in the continuum revealed a systematic shift in phase of the derived angular diameter of 0.02. However, the distance is not affected

because it is linked to the amplitude of the angular diameter curve, which is only slightly changed by the shift effect. They further claim that considering the time-dependence of limb-darkening does not seem to be a priority for the IBW method. The validity of this claim is considered in Section 8.1 and the use of a phase-dependent limb-darkening factor is justified for the wavelength of the observations presented here (696 nm).

In the absence of a CTL intensity distribution computed for a hydrodynamic model of  $\ell$  Car, as done for  $\zeta$  Gem, use has been made of the tabulation of  $\rho_\lambda$  by Davis et al. (2000) computed for the extensive grid of centre-to-limb intensity variations given by Kurucz (1993a,b) for his model atmospheres.

A value of  $[Fe/H] = 0.3$  has been adopted for  $\ell$  Car following Cayrel de Strobel et al. (1997). Taylor (1999) has tabulated 47 values of  $T_{eff}$  and  $\log g$  as a function of phase and these data have been adopted to establish a  $\rho_{696}$  versus phase curve. For each phase tabulated by Taylor a value for  $\rho_{696}$  was interpolated from the Davis et al. (2000) tabulation. A sixth order Fourier series was fitted to the resulting values of  $\rho_{696}$  versus phase (the lowest order to give a smooth and accurate representation of the data; the data has a standard deviation from the fitted curve of 0.00024). The coefficients of the fit were then used to compute values for  $\rho_{696}$  for the phases of the SUSI uniform-disk angular diameter determinations. These values are listed in Table 4 and plotted in Figure 2. Figure 2 also includes the values determined for the Taylor phases and the curve fitted to them. Taylor included estimates of the uncertainties in the values of  $T_{eff}$  and  $\log g$  in her tabulation and from these uncertainties it is estimated that the values of  $\rho_{696}$  in Table 4 are accurate to  $\pm 0.001$ , with the caveat that we are assuming that the Kurucz models upon which Davis et al. (2000) based their tabulation of limb-darkening factors are appropriate for  $\ell$  Car. The mean value of  $\rho_{696}$  for the fitted curve is 1.057.

#### 5.5 The Limb-Darkened Angular Diameters

The uniform-disk angular diameters have been converted to limb-darkened angular diameters ( $\theta_{LD}$ ) in Table 4 using the listed limb-darkening correction factors. The uncertainties in the uniform-disk and limb-darkened angular diameters given in Table 4 do not include the uncertainty in the effective wavelength, which is a systematic uncertainty of  $\pm 0.3\%$ . Its effect on the mean angular diameter and on the distance to  $\ell$  Car will be discussed in Section 8. The uncertainty in the limb-darkened angular diameter in Table 4 does however

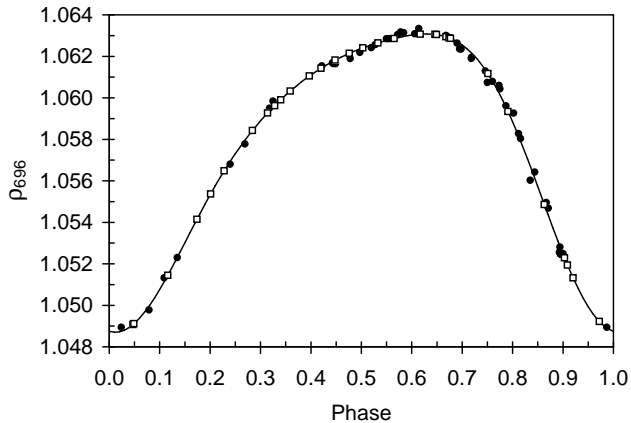


**Figure 2.** Limb-darkening factor  $\rho_{696}$  v. pulsation phase for  $\ell$  Car. The curve is the sixth order Fourier series fit to the filled circles which are the values determined for the phases tabulated by Taylor (1999). The open squares are the values for the epochs of the SUSI determinations of the uniform-disk angular diameters, computed from the coefficients of the Fourier fit. Further details are given in the text.

include the uncertainty in the limb-darkening correction factor.

## 6 THE SPECTROSCOPIC DATA

In order to determine the distance and mean diameter of  $\ell$  Car the radial displacements of the stellar surface as a function of phase are required for combination with the limb-darkened angular diameters. The starting point for establishing the radial displacements is the observed radial velocity curve as a function of phase.

### 6.1 The Radial Velocity Data

The most extensive radial velocity data set is that by Taylor et al. (1997) based on 67 spectra from Mount Stromlo Observatory (MSO) in Australia and 70 spectra from Mount John University Observatory (MJUO) in New Zealand. Early measurements of radial velocity induced spectral line displacements were generally made by line centroid or bisection estimates made by eye (e.g. Dawe 1969) which was the last published velocity curve for  $\ell$  Car prior to Taylor et al. (1997).

Taylor et al. (1997) determined radial velocities by averaging the radial velocities for 19 metallic lines measured by the line-bisector method (Wallerstein et al. 1992) from an average of depths 0.7, 0.8 and 0.9 (continuum at 0.0 and core at 1.0). The MSO and MJUO sets of data were initially phased using the ephemeris of Shobbrook (1992) but Taylor et al. (1997) found a small phase shift between the earliest MJUO observations and later observations and derived a small phase correction to bring all the MSO and MJUO observations into phase alignment. We have adopted their tabulated data that include the phase adjustments with three exceptions. The Julian Dates 2449408.65 and 2450380.57 for MSO data and 2449408.66 for MJUO data

correspond to times during daylight hours so data for these dates have been omitted leaving a total of 134 data points.

Bersier (2002) lists HJDs for 19 radial velocity measurements for  $\ell$  Car but does not give phases. For  $\ell$  Car the maximum difference between HJD and JD is negligible at less than  $3 \times 10^{-5}$  of the pulsation period and has been ignored. Phases have been computed with Shobbrook’s ephemeris and the resulting data are in good phase agreement with the data of Taylor et al. (1997), discussed above, but there is an offset in radial velocity. Kervella et al. (2004b) first noted this and chose ‘to shift the Taylor et al. (1997) data set by  $-1.5 \text{ km s}^{-1}$  to bring all the data on the well established CORAVEL system of Bersier (2002)’. Since the data set of Taylor et al. (1997) is significantly more numerous than that of Bersier (2002) (134 data points versus 19), and the decision has been made to adopt the Taylor et al. (1997) as the basic data set, we have adjusted the Bersier radial velocities. This decision is supported by the work of Kiss (1998) who found that, while ‘CORAVEL measurements have excellent internal accuracy, their absolute values are very uncertain’. The Bersier data, determined by the cross-correlation technique rather than the line-bisector method employed by Taylor et al. (1997), were combined with the Taylor et al. data with a range of offsets for the Bersier radial velocities. For each offset a sixth order Fourier series was fitted over the range in phase from -0.037 to 0.75 (the reasons for the choice of the order of the fit and of the range in phase will be discussed in Section 6.2) and the minimum value of  $\chi^2$  corresponds to the addition of  $2.0 \text{ km s}^{-1}$  to the Bersier data. In view of the resulting good agreement between the Bersier and Taylor et al. data over the whole pulsation cycle including the amplitude of the radial velocity variation, the Bersier data have been accepted in spite of the different technique used for measuring the line shifts.

Petterson et al. (2005) have measured 34 radial velocities at the MJUO and while these are more recent than those of Taylor et al. (1997), the technique for measuring the radial velocities by the line-bisector method is identical. As well as giving the JDs of the observations the authors have listed phases based on an ephemeris by Pel (1976) which are significantly offset from the data of Bersier and Taylor et al. We have computed the phases from the given JDs, using the ephemeris of Shobbrook (1992), and find a small phase offset from the Taylor et al. data suggesting a glitch or period change between the Taylor et al. and the later Petterson et al. observations. In order to establish the optimum phase adjustment the Petterson et al. data were combined with the Taylor et al. data with a range of phase offsets. For each offset a sixth order Fourier series was fitted over the range in phase from -0.037 to 0.75, as in the case of the Bersier radial velocities, and the minimum value of  $\chi^2$  corresponds to the subtraction of 0.02 in phase from the Petterson et al. (2005) data. The adjusted Petterson et al. data are in excellent agreement with the combined Taylor et al. and Bersier radial velocity data with the exception of the five data points for JD 2451163.0392, 2450683.1543, 2450683.8039, 2450684.1304 and 2450684.8105 which all lie several times the quoted uncertainties from the combined Taylor et al., Bersier, and Petterson et al. plot of radial velocity against phase. The Petterson et al. data have been accepted with the exception of the five discrepant points.

**Table 5.** Details of the Fourier series fits to the selected radial velocity data in three ranges in phase.  $N$  is the number of data points in each range in phase,  $N_F$  is the order of the Fourier series fit, and Phase(M) is the phase at which the separate fits were matched. Further details are given in the text.

Section	Phase Range	$N$	$N_F$	Phase(M)
Rising	-0.037 to 0.75	137	6	
Rising to Middle				0.710
Middle	0.701 to 0.896	42	6	
Middle to Falling				0.890
Falling	0.862 to 1.031	38	6	
Falling to Rising				0.015

Nardetto et al. (2006a) have published radial velocities for  $\ell$  Car determined by three different methods of measuring line displacements. These methods differ from those used for the data considered so far and result in a range of amplitudes of the radial velocity curve bracketing the amplitude of the curve determined from the Taylor et al., Bersier and Petterson et al. curve with none of the three agreeing with it. In view of the disagreement with the other three sources the Nardetto et al. (2006a) data have not been included.

## 6.2 The Radial Velocity Curve

Figure 3 shows the assembled radial velocity data versus phase together with the fitted curve. Attempts were made to fit a Fourier series to the assembled data but even with a sixteenth order series the fit was poor in parts. Taylor (1999) overcame this difficulty by fitting a sixth order Fourier fit to the ascending branch of the curve and a ninth order fit to the descending branch. After some experimentation it was found that the good fit shown in Figure 3 could be obtained by dividing the curve into three ranges in phase and making a separate sixth order Fourier series fit to each. The ranges of the fits, which overlap, are listed in Table 5. In each case the reduced  $\chi^2$  values indicated that the published uncertainties in the radial velocities are optimistic. Adopting uncertainties of  $\pm 0.45 \text{ km s}^{-1}$ ,  $\pm 0.50 \text{ km s}^{-1}$ , and  $\pm 1.0 \text{ km s}^{-1}$  for the rising, middle, and falling sections respectively gave reduced  $\chi^2$  values close to unity. The coefficients of the fits were employed to compute radial velocities at intervals of 0.005 in phase over the ranges of the fits and plots were made of the fits in the overlapping regions. The phases for the transitions from one fit to the next were chosen by inspection of these plots and were the phases at which the overlapping fits were closest to each other. For the transition between the rising and middle sections the radial velocities at phase 0.710 were adjusted to an intermediate value to give a smooth transition between the fits on either side. Similarly, for the transition between the middle and falling sections, the radial velocity at phase 0.890 was adjusted and, for the transition between the falling and rising sections, the radial velocity at phase 0.015 was adjusted. The adjustments to the radial velocities were small, averaging  $\sim 0.3\%$  of the mean radial velocities at the transitions. The fits are summarised and the phases at which they were matched are listed in Table 5.

The radial velocity curve shown in Figure 3, assem-

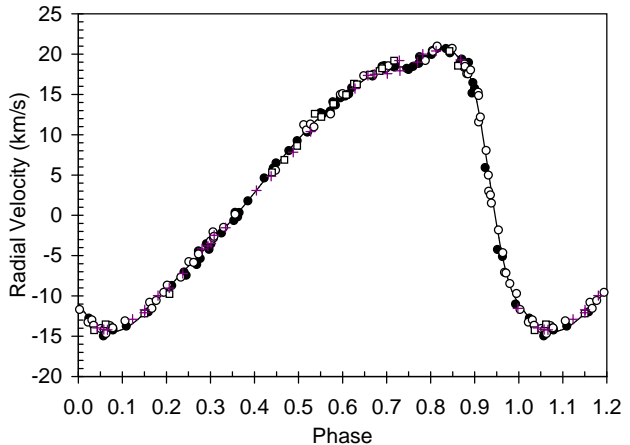


**Figure 3.** The assembled radial velocity curve v. phase for  $\ell$  Car. The line is the fit to the data; filled circles are MSO data from Taylor et al. (1997); open circles are MJUO data from Taylor et al. (1997); open squares are data by Bersier (2002); and crosses are data by Petterson et al. (2005). Details are given in the text.

bled from the Fourier series fits listed in Table 5, has been adopted for the subsequent analysis

## 6.3 The $p$ -Factor

The radial velocity curve in Figure 3 is for the measured radial velocities but does not represent the true radial velocity of the stellar surface since it is a value integrated over the stellar surface. It includes projection and limb-darkening effects that vary from the centre to the limb of the star. These effects depend on spectral line shape, which is not only a function of phase, but is also affected by the velocity structure within the line-forming region and the contributions from the different layers of the atmosphere. Conventionally, in the absence of sufficiently detailed modelling of the stellar atmosphere, the measured radial velocities are multiplied by a constant, known as the  $p$ -factor, to correct them to the radial velocity of the stellar surface. There are a number of issues to be considered in the choice of  $p$  since any error or uncertainty in the value adopted translates directly to the distance determined for the Cepheid when the spectroscopic and interferometric data are combined.

The evaluation of  $p$ -factors is generally derived from model stellar atmosphere models but Mérand et al. (2005) have presented a measured value of  $1.27 \pm 0.06$  for the  $p$ -factor for  $\delta$  Cep based on interferometric measurements with the CHARA Array and on the Hubble Space Telescope parallax (Benedict et al. 2002). The accuracy is limited by the parallax and the authors conclude that theoretical studies using realistic hydrodynamical codes are needed.

The literature dealing with the theoretical evaluation of the  $p$ -factor from model atmosphere studies is extensive but with no clear results applicable to  $\ell$  Car. While Sabbey et al. (1995) claim that the phase dependence of  $p$  increases the Baade-Wesselink (BW) radius by  $\sim 4 - 6\%$ , depending on the constant value of  $p$  used for comparison, Nardetto et al. (2004) claim that their choice of a constant  $p$ -factor for the Interferometric Baade-Wesselink method (IBW), compared

to a time-dependent one, leads to a systematic error of the order of only 0.2% in the final distance determination for  $\delta$  Cep.

The projection factor is also sensitive to the centre-to-limb intensity distribution or limb darkening, but it is not clear whether a mean value for the limb-darkening is adequate or whether a phase dependence is significant for the  $p$ -factor. However, it is clear that the phase dependence of limb darkening is significant for the conversion of uniform-disk angular diameters to limb-darkened angular diameters at 696 nm, as mentioned in Section 5.4 and justified in Section 8.1.

In most cases more detailed modelling and, in particular, the hydrodynamic modelling in spherical geometry that predicts a phase dependence of  $p$  has been done for a particular Cepheid, most commonly  $\delta$  Cep or  $\zeta$  Gem, and the results are not in a form that can be scaled to other Cepheids. The concluding recommendation of these studies is generally that each Cepheid should be individually modelled. This is not within the scope of our programme and we have therefore decided to use a fixed value but to make available all the relevant data to enable the results to be updated by others when improved values for  $p$ , or an appropriate model for  $\ell$  Car have been developed.

A brief summary and discussion of the fixed values of  $p$  adopted for  $\ell$  Car in the literature is appropriate at this point. As noted by Taylor et al. (1997) the value of  $p$  depends not only on the technique used to measure the radial velocities, but also upon the strength of the lines chosen and their wavelengths. Taylor et al. (1997) adopted a value of  $1.38 \pm 0.03$  (Albrow & Cottrell 1994) but revised their results (Taylor & Booth 1998) using  $p = 1.39 - 0.03 \log P = 1.34$  (Hindsley & Bell 1986; Gieren, Barnes & Moffett 1993). Kervella et al. (2004b), in a comparison of the interferometric and surface brightness techniques, used the same formula with  $p = 1.343$  for  $\ell$  Car. In this comparison they only considered radial velocity points in the phase interval 0.0 to 0.8 following Storm et al. (2004). However, Kervella et al. (2004a) adopted a value of 1.36 for  $p$  for all the 7 Cepheids in their programme which included  $\ell$  Car and justified it on the grounds that Burki, Mayor & Benz (1982) had shown that this value was appropriate for the radial velocity measurements by Bersier (2002) that they had used. Nardetto et al. (2007) have used a hydrodynamic model of  $\ell$  Car to validate a spectroscopic method of determining the  $p$ -factor in which it was divided into three sub-concepts. While their work is not directly applicable to our data, because it was restricted to a single specific spectral line and the method employed for measuring the line differed from that for the data we are using, they derived a value of  $1.27 \pm 0.02$  for  $p$ . Groenewegen (2007) has evaluated a relationship between the  $p$ -factor and pulsation period based on five Cepheids with interferometrically measured angular diameter variations and known distances taken from the literature. Based on a total of seven stars with periods in the range 5-35 days it is claimed that there is no evidence for a period dependence of the  $p$ -factor although values found range from 1.193 to 1.706, albeit with large uncertainties in the majority of cases. For  $\ell$  Car the  $p$ -factor is found to be  $1.193 \pm 0.058 \pm 0.120$  based on the distance of  $498 \pm 50$  pc determined by Benedict et al. (2007) with the Hubble Space Telescope Fine Guidance Sensors. The first

uncertainty is from the fitting process and the second is due to the uncertainty in the distance. The majority of distance determinations to  $\ell$  Car to date, which are listed in Table 6 and include the distance determined here, suggest a larger value for the distance to  $\ell$  Car, implying a larger value for the  $p$ -factor of the order of 1.29 if determined by the approach employed by Groenewegen. Based on the five Cepheids analysed, which had interferometrically determined angular diameters and distances, Groenewegen (2007) concluded that a constant value of  $p = 1.25 \pm 0.05$  was appropriate. But, as has been discussed, at least in the case of  $\ell$  Car a larger value is indicated.

To summarise, there is no agreement on the optimum fixed value of the  $p$ -factor to use although it is clear that it depends on the individual Cepheid and on the details of the observing and analysis techniques used for both spectroscopy and interferometry. Faced with these difficulties we have adopted a constant value of  $1.30 \pm 0.05$ . The influence of this decision on the mean diameter and distance of  $\ell$  Car will be discussed in Section 8.

#### 6.4 The Radial Displacement Curve

Integration of the radial velocity curve shown in Figure 3 gave the radial velocity of the centre of mass  $V_\gamma$  equal to  $+4.13 \pm 0.01 \text{ km s}^{-1}$  where the uncertainty has been estimated using the bootstrapping method. This differs from the value of  $+4.21 \pm 0.01 \text{ km s}^{-1}$  given by Taylor et al. (1997) but is based on the assembly of a larger body of radial velocity data.

The radial displacement of the stellar surface in solar radii  $\Delta R(\phi)$ , as a function of phase  $\phi$ , was found by integrating the radial velocity  $V_{\text{RV}}(\phi)$ , after correction for  $V_\gamma$ , using

$$\Delta R(\phi) = -\frac{pP}{R_\odot} \int (V_{\text{RV}}(\phi) - V_\gamma) d\phi \quad (4)$$

where  $P$  is the pulsation period in seconds and  $R_\odot$  is the solar radius in km.

The integrations were made at intervals in phase of 0.005 and the resulting values of radial displacement, after the determination and subtraction of the mean value, were fitted with a Fourier series. Series of increasing order were fitted and it was found that the reduced  $\chi^2$  value for the fits had a minimum value for a sixteenth order fit. This has been adopted for the subsequent analysis. The uncertainty in the radial displacements has been evaluated following Taylor et al. (1997) using the expression by Balona (1977):

$$\sigma(\text{RD}) = \frac{pP\sigma(\text{RV})}{2R_\odot\sqrt{N}} \quad (5)$$

where  $\sigma(\text{RD})$  is the uncertainty in radial displacement in solar radii,  $P$  is the pulsation period in seconds,  $\sigma(\text{RV})$  is the standard deviation of the radial velocities about the fitted curve ( $\sigma(\text{RV}) = 0.6 \text{ km s}^{-1}$ ),  $R_\odot$  is the solar radius in km, and  $N$  is the number of observations. Substitution in equation (5) gives  $\sigma(\text{RD}) = 0.13 R_\odot$  (less than 0.4% of the total radial displacement due to the Cepheid pulsation).



## 7 THE COMBINATION OF INTERFEROMETRIC AND SPECTROSCOPIC DATA

The relationship between the limb-darkened angular diameter  $\theta_{\text{LDobs}}$  and the radial displacement of the Cepheid surface is given by

$$\theta_{\text{LDobs}}(\phi_i) = \overline{\theta_{\text{LD}}} + 9.298 \left( \frac{\Delta R(\phi_i)}{d} \right) \quad \text{mas} \quad (6)$$

where  $\overline{\theta_{\text{LD}}}$  is the mean limb-darkened angular diameter (the limb-darkened angular diameter at zero displacement),  $\Delta R(\phi_i)$  is the radial displacement in solar radii for the  $i$ th observation at phase  $\phi_i$ ,  $d$  is the distance in pc, and the constant converts the term in parentheses into mas using values for the solar radius and parsec in metres from Cox (1999).

A weighted linear least squares fit has been made to  $\theta_{\text{LD}}(\phi_i)$  versus  $\Delta R(\phi_i)$  to determine  $\overline{\theta_{\text{LD}}}$  and  $d$  for  $\ell$  Car. A small phase shift was found between the angular diameter and radial velocity data, which is not surprising since the epoch of the first SUSI observation was more than 40 pulsation periods after the last radial velocity observation. The phase offset was established by repeating the fit with a range of phase offsets to find the minimum value of reduced  $\chi^2$  for the fit. The phase offset was found to be a correction of  $-0.0635 \pm 0.015$  to the phases of the radial displacements relative to the phases of the angular diameters. The fit using this offset gives the mean limb-darkened angular diameter of  $\ell$  Car equal to  $2.981 \pm 0.005$  mas and the distance to  $\ell$  Car equal to  $523 \pm 15$  pc. The observational data are shown in Figure 4 with the fitted line.

In Section 5.3 the apparent inconsistency of the uniform-disk angular diameter of  $\iota$  Car was discussed and the possibility of increasing it to  $1.77 \pm 0.12$  mas was proposed although all the analysis to this point has been carried out with our estimate for its angular diameter of  $1.55 \pm 0.12$  mas. In order to investigate the effect of increasing the angular diameter the analysis to this point has been repeated with the angular diameter of  $\iota$  Car equal to  $1.77 \pm 0.12$  mas. The results are: phase offset  $-0.064 \pm 0.001$ , mean limb-darkened angular diameter of  $\ell$  Car equal to  $2.999 \pm 0.005$  mas and the distance to  $\ell$  Car equal to  $526 \pm 15$  pc.

At this point it is stressed that the uncertainties are those given by the fits. However, it can be seen that the change in the angular diameter of  $\iota$  Car has essentially negligible effect on the distance determination compared with the uncertainty in the distance, but does increase the mean angular diameter by more than three times the formal uncertainty from the fits. The difference in the mean angular diameter and systematic uncertainties that have not been considered so far are discussed in Section 8.

The limb-darkened angular diameters versus phase for  $\ell$  Car, assuming the angular diameter of  $\iota$  Car equal to  $1.55 \pm 0.12$  mas, are shown in Figure 5 together with the limb-darkened angular diameter versus phase curve computed for the fit to limb-darkened angular diameter versus radial displacement.

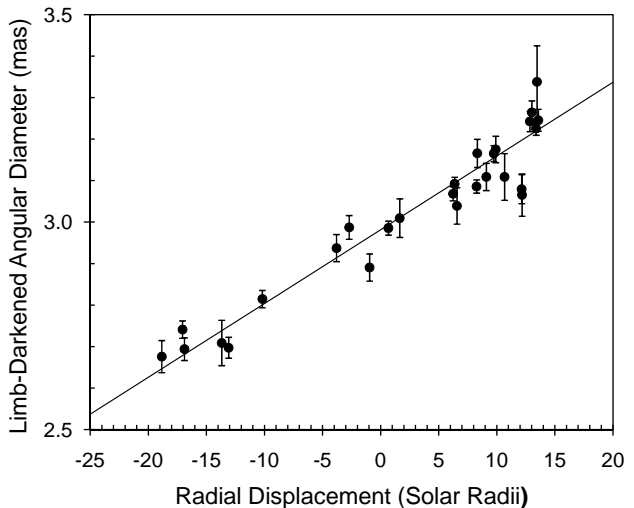


**Figure 4.** The limb-darkened angular diameter versus radial displacement for  $\ell$  Car. The filled circles with error bars are the observed values of limb-darkened angular diameter from Table 4 and the line is the fit to angular diameter versus radial displacement using equation (6). Further details are given in the text.

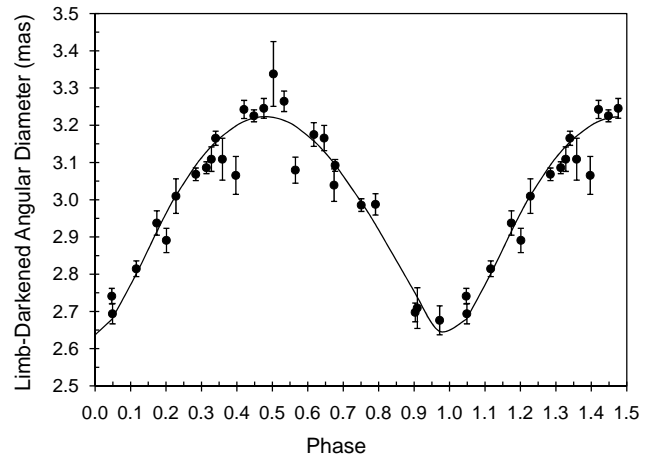


**Figure 5.** The limb-darkened angular diameter versus phase for  $\ell$  Car. The filled circles with error bars are the observed values of limb-darkened angular diameter from Table 4 and the line is the computed limb-darkened angular diameter versus phase from the fit to angular diameter versus radial displacement using equation (6). The data points and curve in the phase interval 0–0.5 have been repeated for the phase interval 1.0–1.5. Further details are given in the text.

## 8 DISCUSSION

In Section 7 two values were presented for the mean limb-darkened angular diameter of  $\ell$  Car:  $2.981 \pm 0.005$  mas for the uniform-disk angular diameter of the calibrator  $\iota$  Car equal to  $1.55$  mas and  $2.999 \pm 0.005$  mas for  $\iota$  Car equal to  $1.77$  mas. Increasing the uniform-disk angular diameter of  $\iota$  Car produced greater consistency between the three calibrators, as discussed in Section 5.3, but the change was arbitrary and we cannot be certain that the larger value is correct. We

therefore adopt the mean of the two results and assign an uncertainty to cover the uncertainties of the two values. In addition there is a systematic uncertainty due to the uncertainty in the effective wavelength of  $\pm 0.3$  per cent. Thus the final value for the mean limb-darkened angular diameter of  $\ell$  Car, with the systematic uncertainty in parentheses, is  $\overline{\theta_{LD}} = 2.990 \pm 0.014$  ( $\pm 0.009$ ) mas. This value is in excellent agreement with the only other direct interferometric determination by Kervella et al. (2004a) of  $2.988 \pm 0.012$  mas.

The corresponding two values for the distance presented in Section 7, namely  $523 \pm 15$  pc and  $526 \pm 15$  pc, are in good agreement and we adopt  $525 \pm 16$  pc for the distance. There are two systematic uncertainties in the distance due to the effective wavelength ( $\pm 0.3$  per cent) and the  $p$ -factor ( $\pm 3.8$  per cent). The value for the distance to  $\ell$  Car, with the systematic uncertainty in parentheses, is  $525 \pm 16$  ( $\pm 20$ ) pc. Combining the uncertainties quadratically gives the distance as  $525 \pm 26$  pc.

### 8.1 A Constant versus a Phase-Dependent Limb-Darkening Factor

The limb-darkening factor for converting uniform-disk angular diameters to limb-darkened angular diameters is expected to vary with pulsation phase and we have taken this into account as discussed in Section 5.4. However, the question has been asked as to whether this was necessary and would a constant value, equal to the mean value taken from the curve in Figure 2, have given different results. To examine this, the entire analysis has been repeated using the mean value of the limb-darkening factor of 1.057, given in Section 5.4, in place of the phase-dependent values given in Table 4.

The mean limb-darkened angular diameter was found to be unchanged as expected. The mean limb-darkened angular diameter of  $\ell$  Car was  $2.979 \pm 0.017$  mas for the uniform-disk angular diameter of the calibrator  $\iota$  Car equal to 1.55 mas and  $2.997 \pm 0.017$  mas for  $\iota$  Car equal to 1.77 mas, where the statistical and systematic uncertainties have been combined quadratically. In each case the values are slightly smaller than the values for the phase-dependent limb-darkening factor (0.002 mas) but this is a result of the rounding of the mean value of the limb-darkening factor.

The distance to  $\ell$  Car is changed because the mean limb-darkening factor results in a smaller angular pulsation amplitude ( $0.525 \pm 0.018$  mas compared with  $0.560 \pm 0.018$  mas). The corresponding values for the distance are  $559 \pm 17$  pc and  $561 \pm 17$  pc compared with  $523 \pm 15$  pc and  $526 \pm 15$  pc for the phase-dependent limb-darkening factor. The mean of the two values in each case is  $560 \pm 18$  pc and  $525 \pm 16$  pc. The difference is significant and justifies the use of the phase-dependent limb-darkening factor. Kervella et al. (2004b) neglected the phase dependence of the limb-darkening factor in their study of  $\ell$  Car. Their decision was based on the estimate by Marengo et al. (2003) that the variation would be less than 0.3 per cent peak to peak in the  $H$  band for  $\zeta$  Gem and the fact that it would be even less in the  $K$  band. At 696 nm the limb-darkening factor varies by more than 1.3 per cent, as shown in Figure 2, and cannot be ignored.

### 8.2 A Comparison of Distance and Radius Determinations

Table 6 lists recent values for the distance to  $\ell$  Car from the literature together with the value determined in this work for a phase-dependent limb-darkening factor. For the latter the statistical and systematic uncertainties have been combined quadratically. The value by Taylor & Booth (1998) using the BE method, which succeeds the value by Taylor et al. (1997), has an unrealistic published uncertainty of  $\pm 4$  pc because systematic effects have not been taken into account. Gieren, Fouqué & Gómez (1997) have shown that a systematic uncertainty of the order of  $\pm 3$  per cent should be taken into account for the surface brightness method and the uncertainty for the Taylor et al. (1997) distance in Table 6 has been increased to include this additional uncertainty. It is noted that the values by Kervella et al. (2004b) using the IBW and IRSB methods, and by Barnes et al. (2005) by the IRSB method, do not include an allowance for the systematic uncertainty in the  $p$ -factor adopted.

The distance values in Table 6 that involve the  $p$ -factor have used different values to that adopted here and, while it is recognised that different values *may* be appropriate for different methods, a column has been added to the table with the distances scaled to a common value of  $p = 1.30 \pm 0.05$ . The uncertainties associated with this column have been increased to combine quadratically the uncertainty in the  $p$ -factor with the published uncertainty where appropriate. The uncertainty in the value by Taylor et al. (1997) has been increased further as Gieren et al. (1997) included a smaller uncertainty in the  $p$ -factor ( $\pm 2.5\%$ ) in their evaluation of the systematic uncertainty. Examination of the distances for the common  $p$ -factor show excellent agreement for all values.

Columns for the mean radius of  $\ell$  Car are included in Table 6, one for the published values and one for a common  $p$ -factor, following the same approach as for the distance. The uncertainty in the limb-darkened angular diameter for the IBW determinations has been taken into account although it is negligible compared with the uncertainty in the distance. Examination of the mean radii for the common  $p$ -factor also show excellent agreement for all values.

The mean total range in limb-darkened angular diameter has been taken from the curves fitted to limb-darkened angular diameter versus radial displacement for the two values of uniform-disk angular diameter for the calibrator  $\iota$  Car. It is  $0.560 \pm 0.018$  mas, which corresponds to  $18.7 \pm 0.6$  per cent of the mean stellar diameter.

## 9 CONCLUSION

The measurement of the angular pulsations of Cepheid variables and the combination with spectroscopically determined radial displacements of the stellar atmospheres was one of the key programmes for which SUSI was developed. Only recently has adequate sensitivity been achieved for this programme to be undertaken and the first results are those for  $\ell$  Car presented here.

The angular pulsation of  $\ell$  Car has been measured with good cover in pulsation phase and careful attention has been paid to uncertainties in the measurements, in the adopted calibrator angular diameters, in the projected

**Table 6.** The distance to  $\ell$  Car.  $p$  is the  $p$ -factor, the column headed ID contains acronyms for the methods employed with the key at the foot of the table, and the key to the numbered references is also at the foot of the table. Further details are given in the text.

Distance	Radius	$p$	ID	Distance	Radius	Reference
(pc)	( $R_{\odot}$ )			for $p = 1.30$	for $p = 1.30$	
				(pc)	( $R_{\odot}$ )	
550±17	173±5	1.34	BE	534±22	168±7	1
566 <sup>+24</sup> <sub>-19</sub>	182 <sup>+8</sup> <sub>-7</sub>	1.343	IBW	548 <sup>+30</sup> <sub>-27</sub>	176 <sup>+10</sup> <sub>-9</sub>	2
560±23	179±7	1.343	IRSB	542±30	173±10	2
559±19	179.9±6.4	1.343	IRSB-Bay	541±27	174±9	3
485±64	—	—	RH	—	—	4
498±50	—	—	HST	—	—	5
525±26	168.8±8.2	1.30	IBW	525±26	169±8	This work

Key to ID acronyms: BE - Barnes-Evans; IBW - Interferometric Baade-Wesselink; IRSB - Infrared Surface Brightness; IRSB-Bay - Infrared Surface Brightness (Bayesian); RH - Revised Hipparcos Parallax; HST - Hubble Space Telescope Fine Guidance Sensors.

Key to References: 1 - Taylor & Booth (1998); 2 - Kervella et al. (2004b); 3 - Barnes et al. (2005); 4 - van Leeuwen (2007); 5 - Benedict et al. (2007).

value of  $V^2$  at zero baseline, and to systematic effects. A phase-dependent limb-darkening factor, to convert uniform-disk angular diameters to limb-darkened angular diameters, was established based on Kurucz model atmospheres and its use, rather than a fixed mean value for the limb-darkening factor, was justified for 696 nm. The resulting mean limb-darkened angular diameter is  $2.990 \pm 0.017$  mas (i.e.  $\pm 0.6$  per cent) with a maximum-to-minimum amplitude of  $0.560 \pm 0.018$  mas corresponding to  $18.7 \pm 0.6$  per cent in the mean stellar diameter. The projected value of  $V^2$  at zero baseline shows no evidence at 696 nm of the circumstellar envelope observed in the  $N$  and  $K$  bands by Kervella et al. (2006).

A radial displacement curve has been computed from carefully selected radial velocity measurements from the literature and this has been combined with the interferometric data to determine the mean radius and distance to  $\ell$  Car. The value for the distance is  $525 \pm 26$  pc and the mean radius is  $169 \pm 8 R_{\odot}$ . These values have been compared with values in the literature and excellent agreement is found, particularly when all values are reduced to a common  $p$ -factor.

The uncertainty in the  $p$ -factor is a major contributor to the uncertainties in the distance and mean radius. The SUSI data may be useful in the future if  $\ell$  Car specific hydrodynamic spherical models are generated that consider the possibility of a phase-dependence of limb-darkening and the  $p$ -factor as discussed, for example, by Sasselov & Karovska (1994) and Marengo et al. (2002). To facilitate such possible applications the calibrated  $V^2$  values may be obtained from the lead author (JD).

## 10 ACKNOWLEDGEMENTS

The SUSI programme is funded jointly by the Australian Research Council and the University of Sydney. MJI acknowledges the support of an Australian Postgraduate Award, APJ and JRN the support of University of Sydney Postgraduate Awards and APJ the support of a Denison Postgraduate Award during the course of this work. We are grateful to the referee who made a number of suggestions that have helped clarify and justify the approach we have adopted in

our analysis. This research has made use of the SIMBAD data base, operated at CDS, Strasbourg, France.

## REFERENCES

- Albrow M.D., Cottrell P.L., 1994, MNRAS, 267, 548  
Balona L. A., 1977, MNRAS, 178, 231  
Barnes III, T. G., Storm J., Jefferys W. H., Gieren W. P., Fouqué P., 2005, ApJ, 631, 572  
Benedict G. F. et al., 2002, AJ, 124, 1695  
Benedict G. F. et al., 2007, AJ, 133, 1810  
Berdnikov L. N., Turner D. G., 2004, A&AT, 23, 253  
Bersier D., 2002, ApJS, 140, 465  
Burki G., Mayor M., Benz W., 1982, A&A, 109, 258  
Caytel de Strobel G., Soubiran C., Friel E. D., Ralite N., François P., 1997, A&AS, 124, 299  
Cox A. N. (ed.), 1999, Allen's Astrophysical Quantities (Fourth Edition), Springer-Verlag, New York  
Davis J., 1999, in Hearnshaw J. B., Scarfe C. D., eds., Proc. IAU Coll. 170, Precise Stellar Radial Velocities. ASP Conf. Series 185, p. 390  
Davis J., Tango W. J., Booth A. J., ten Brummelaar T. A., Minard R. A., Owens, S. M., 1999, MNRAS, 303, 773  
Davis J., Tango W. J., Booth A. J., 2000, MNRAS, 318, 387  
Davis J. et al., 2007a, PASA, 24, 138  
Davis J., Ireland M. J., Jacob A. P., North J. R., Owens S. M., Robertson J. G., Tango W. J., Tuthill P. G., 2007b, in Richichi A., Delplancke F., Parese F., Chelli A., eds., The Power of Optical/IR Interferometry: Recent Scientific Results and 2nd Generation Instrumentation. ESO Astrophysics Symposia, p. 105. Springer-Verlag, Berlin  
Dawe J.A., 1969, MNRAS, 145, 377  
Gieren W.P., Barnes T.G., Moffett T.J., 1993, ApJ, 418, 135  
Gieren W. P., Fouqué P., Gómez M., 1997, ApJ, 488, 74  
Groenewegen M. A. T., 2007, A&A, 474, 975  
Hanbury Brown R., Davis J., Allen L. R., 1974, MNRAS, 167, 121  
Hindsley R.B., Bell R.A., 1986, PASP, 98, 881  
Jacob A. P., 2008, Observations of Three Cepheid Stars with SUSI, PhD thesis, University of Sydney

- Kervella P., Nardetto N., Bersier D., Mourard D., Coudé du Foresto V., 2004a, *A&A*, 416, 941
- Kervella P., Fouqué P., Storm J., Gieren W. P., Bersier D., Mourard D., Nardetto N., Coudé du Foresto V., 2004b, *ApJ*, 604, L113
- Kervella P., Mérand A., Perrin G., Coudé de Foresto V., 2006, *A&A*, 448, 623.
- Kiss L. L., 1998, *MNRAS*, 297, 825
- Kurucz R. L., 1993a, Limbdarkening for 2kms<sup>-1</sup> grid (No. 13):[+1.0] to [-1.0], Kurucz CD-ROM No. 16
- Kurucz R. L., 1993b, Limbdarkening for 2kms<sup>-1</sup> grid (No. 13):[+0.0] to [-5.0], Kurucz CD-ROM No. 17
- Lane B. F., Kuchner M. J., Boden A. F., Creech-Eakman M., Kulkarni S. R., 2000, *Nature*, 407, 485
- Lane B. F., Creech-Eakman M. J., Nordgren T. E., 2002, *ApJ*, 573, 330
- Marengo M., Sasselov D.D., Karovska M., Papaliolios, C., 2002, *ApJ*, 567, 1131
- Marengo M., Karovska M., Sasselov D.D., Papaliolios C., Armstrong J.T., Nordgren T.E., 2003, *ApJ*, 589, 968
- Mérand A. et al., 2005, *A&A*, 438, L9
- Mérand A. et al., 2006, *A&A*, 453, 155
- Mérand A. et al., 2007, *ApJ*, 664, 1093
- Mozurkewich D. et al., 2003, *AJ*, 126, 2502
- Nardetto N., Fokin A., Mourard D., Mathias Ph., Kervella P. Bersier D., 2004, *A&A*, 428, 131
- Nardetto N., Mourard D., Kervella P., Mathias Ph., Mérand A., Bersier D., 2006a, *A&A*, 453, 309
- Nardetto N., Fokin A., Mourard D., Mathias Ph., 2006b, *A&A*, 454, 327
- Nardetto N., Mourard D., Mathias Ph., Fokin A., Gillet D., 2007, *A&A*, 471, 661
- Nardetto N., Groh G. H., Kraus S., Millour F., Gillet D., 2008, *A&A*, 489, 1263
- Pel, J.W., 1976, *A&AS*, 24, 413
- Petterson O. K. L., Cottrell P. L., Albrow M. D., Fokin A., 2005, *MNRAS*, 362, 1167
- Sabbey C.N. et al., 1995, *ApJ*, 446, 250
- Sasselov D. D., Karovska M., 1994, *ApJ*, 432, 367
- Shobbrook R. R., 1992, *MNRAS*, 255, 486
- Storm J., Carney B.W., Gieren W.P., Fouqué P. Latham D.W., Fry A.M., 2004, *A&A*, 415, 531
- Szabados L., 1989, *Commun. Konkoly Obs.*, 94, 3
- Taylor M. M., 1999, *Analysis of Cepheid spectra*, PhD thesis, University of Sydney
- Taylor M. M., Albrow M. D., Booth A. J., Cottrell P. L., 1997, *MNRAS*, 292, 662
- Taylor M. M., Booth A. J., 1998, *MNRAS*, 298, 594
- van Leeuwen F., Feast M. W., Whitelock P. A., Laney C. D., 2007, *MNRAS*, 379, 723
- Wallerstein G., Jacobsen T.S., Cottrell P.L., Clark M., Albrow M., 1992, *MNRAS*, 259, 474